Evaluation of Liquefaction Triggering Resistance and Deformation Accumulation in Laminated Sand and Clay Deposits

Panagiota Tasiopoulou, Amalia Giannakou & Jacob Chacko
Fugro
Sjoerd de Wit
Shell Global Solutions International B.V.

ABSTRACT
As part of dynamic stability evaluations of earth embankments founded on laminated sand and clay deposits, the need to characterize their cyclic resistance became critical for the assessment of the embankment behavior and subsequent decisions on liquefaction mitigation measures. Due to the lack of experimental and case history data on the effective stress behavior of such deposits, advanced laboratory tests on high quality undisturbed samples and numerical simulations using advanced constitutive models were performed to gain insight into liquefaction triggering and post-liquefaction accumulation of deformations under level and sloping ground conditions of such formations. Results indicated that the presence of clay laminations within sand deposits tends to increase the liquefaction triggering resistance of such deposits which are typical of tidal and alluvial depositional environments. Numerical analyses results also indicated that void redistribution effects, often related to strain localization effects, tend to be reduced as the thickness of sand layers decreases, or as the percentage of clay interlayers increases.

1 INTRODUCTION

Performance based concepts are increasingly used in earthquake engineering design practice. Nonlinear deformation analyses, involving dynamic finite element or finite difference methods, are frequently used for evaluating the effects of liquefaction on embankment dams and other major soil and soil-structure systems during earthquakes.

In engineering practice, the response of a geotechnical system to strong ground motion is typically evaluated by means of empirical equations developed using either simplified system models or available observations from adequately well documented case histories. Despite their ease of use, simplified empirical models may be overly simplistic in characterizing the response of complex systems and may not capture important phenomena associated with earthquake problems. In the context of performance based design, numerical analyses combined with advanced numerical testing for the calibration of advanced constitutive models can offer an alternative, refined response model, compared to simplified algebraic equations.

Existing simplified procedures (Youd et al 2001, Moss et al 2003, Idriss and Boulanger, 2008; Boulanger and Idriss, 2014) used for liquefaction assessment mainly focus on evaluating liquefaction triggering and post-liquefaction residual strength of sands based on in situ tests (i.e. CPT tip resistance or SPT blowcounts). In intertidal or alluvial environments, however, coarse-grained materials are frequently encountered within thinly layered deposits comprising alternating thin laminations of sands and clays. (see Figure 1). In such types of deposits liquefaction assessment based on empirical correlations with CPT tip resistance may not be applicable due to the effect of the clay layers on the CPT tip resistance measured within the thin “sandwiched” sand layers (i.e. on the order of 10 to 20 cm thick).

As part of dynamic stability evaluations of earth embankments founded on laminated sand and clay deposits, the need to characterize their cyclic resistance became critical for the assessment of embankment behavior and subsequent decisions on liquefaction mitigation measures. Due to the lack of experimental and case history data on the effective stress behavior of such deposits, advanced laboratory tests on high quality undisturbed samples and numerical simulations using advanced constitutive models were performed to gain insight on liquefaction triggering and post-liquefaction accumulation of deformations under level and sloping ground conditions. These results provided the basis for the selection of representative properties and calibration of constitutive models used in 2D dynamic stability numerical evaluations of earth embankments founded on laminated deposits.

Figure 1. Tubes of laminated deposits with alternating thing layers of sand and clay.

2 ADVANCED CYCLING TESTING

A series of stress controlled Cyclic Direct Simple Shear (CDSS) and Cyclic Triaxial (CTX) tests was performed on "undisturbed" samples from laminated deposits. The purpose of the advanced cyclic testing program was to evaluate the liquefaction triggering resistance and post-liquefaction shear deformation potential of the laminated tidal deposits. The cyclic test results were used to evaluate the resistance to liquefaction triggering of individual sand layers within the laminated deposits where CPT tip resistance may have been impacted by the presence of adjacent soft layers and to calibrate nonlinear effective-stress constitutive models that were used to simulate the composite behavior of laminated deposits under earthquake loading in numerical evaluations.

Individual sand layers within the tidal deposits were targeted for the stress-controlled CDSS tests due to the small size of the specimen (i.e. ~ 3 cm), while interlayered sand and clay materials were targeted for CTX tests where specimen size (i.e. ~ 18 cm) is large relative to the interlayer thickness (typically 1-2 cm thick). However, where the layers were thin laminated sand and clay samples were also tested in CDSS tests.

Multi-Sensor Core Logging (MSCL-S) and X-ray radiography was initially performed on select tubes to identify suitable undisturbed subsamples for advanced cyclic testing. Typical examples of CDSS and CTX sample selection from MSCL-S and X-ray results are shown on Figure 2. On the X-ray results shown on Figure 2 lower density fine-grained layers are lighter (closer to white) and higher density coarse-grained layers are darker (typically grey or almost black).

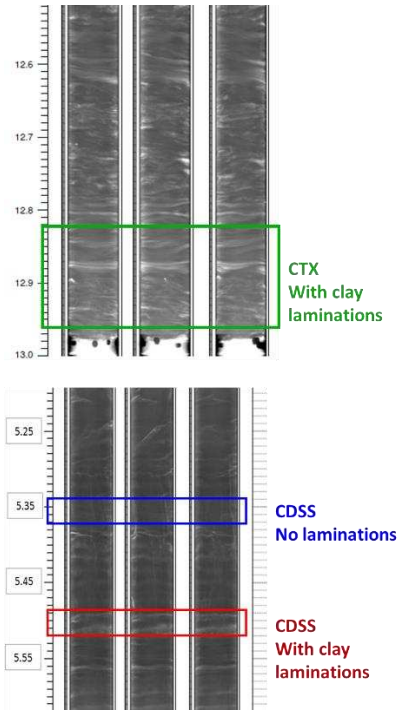

Figure 2. Example sample selection for CDSS and CTX testing based on X-ray radiography. Lower density fine-grained layers are lighter (closer to white) and higher density coarse-grained layers are darker (typically grey or almost black).

Figure 3 depicts the interpreted liquefaction resistance curves obtained from:1) CDSS tests on uniform sand samples (blue curve); and 2) laminated sand and clay samples (red curve); and 3) from CTX tests on laminated sand and clay samples (green curve). Liquefaction triggering was considered to have occurred at 3 percent Single Amplitude shear strain for the CDSS tests and 1.5% Single Amplitude axial strain for the CTX tests. CSR for CDSS tests is defined as the ratio of shear stress amplitude over the initial vertical effective stress, while CSR for CTX tests is equal to the difference between the maximum and minimum principal stresses divided by two, over the initial mean effective stress. As shown on Figure 3 the presence of clay laminations in the samples (red and green curves) leads to an increase in liquefaction triggering resistance compared to a uniform sand sample (blue curve). Tests were performed at a cyclic frequency of 1Hz.

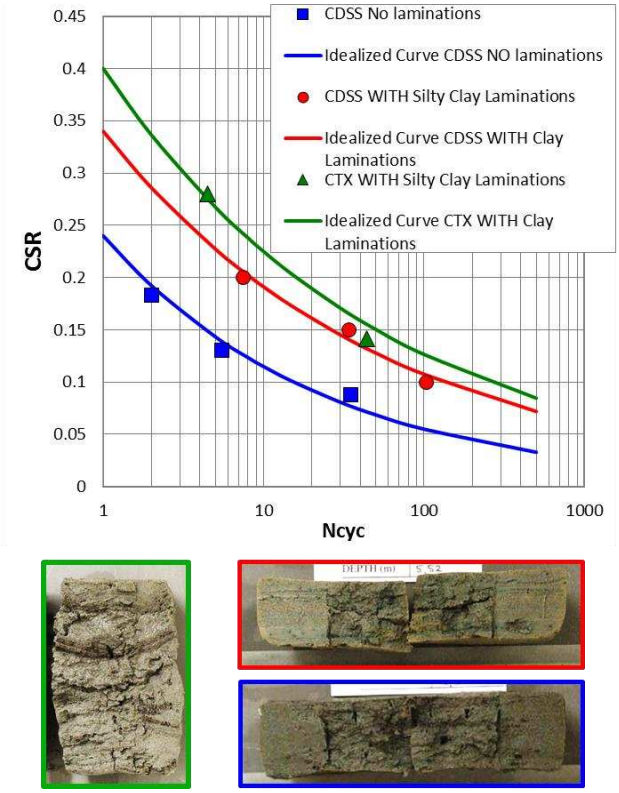

Figure 3. Liquefaction resistance curves obtained from laboratory cyclic testing. The characteristic sample photos below the graph correspond to each curve.

3 NUMERICAL INVESTIGATION OF EFFECTS OF CLAY LAMINATIONS IN SAND DEPOSITS

In addition to advanced cyclic tests, numerical simulations were performed with FLAC2D (Itasca 2011) using advanced constitutive models to simulate the sand layer behavior while also explicitly modeling the clay

laminations. Analyses were performed both at a sample level under laboratory loading conditions (undrained conditions-no flow), as well as at a system level under earthquake loading (flow is allowed). The numerical investigation intended to shed light on the response of laminated soils in terms of liquefaction triggering, post-liquefaction deformation accumulation under sloping ground conditions, and void redistribution effects.

3.1 Constitutive Model Calibration for Uniform Sand Layers

UBCSAND (Beaty and Byrne 1998) and PM4Sand (Boulanger and Ziotopoulou, 2013; Ziotopoulou and Boulanger, 2013) constitutive models were calibrated in order to capture soil triggering and shear strain accumulation behavior for both level (no-bias) and sloping ground (bias) conditions following methodologies described in Giannakou et al (2011).

A number of stress-controlled Cyclic Direct Simple Shear (CDSS) tests were performed with and without static bias on uniform sand samples. Figure 4 presents shear stress-strain loops and stress paths (left illustration) from stress-controlled cyclic simple shear tests on a uniform sand sample for no initial static bias, together with stress-strain loops and stress paths derived from the calibrated UBCSAND and PM4Sand models. Figure 5 presents shear stress-strain loops and stress paths (left illustration) from stress-controlled cyclic simple shear tests on a uniform sand sample for initial static bias equal to 0.2, together with stress-strain loops and stress paths derived from the calibrated UBCSAND and PM4Sand models.

The reasonable comparison between observed and simulated behavior suggests that the calibrated constitutive models can adequately simulate cyclic soil behavior at the element level both in terms of liquefaction triggering and in terms of post-liquefaction shear strain accumulation.

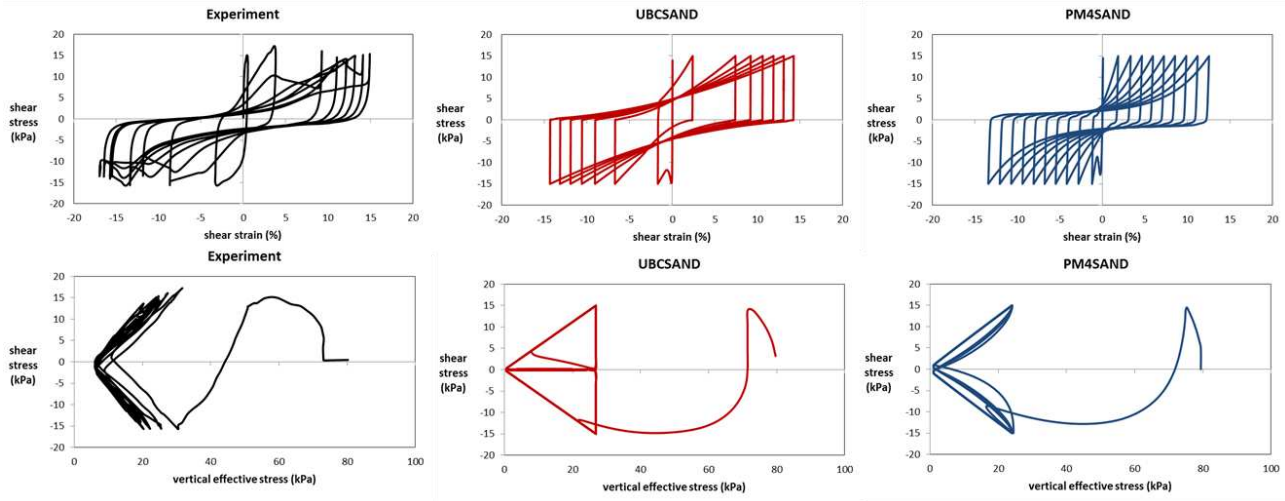

Figure 4. Comparison between experimental and numerical results on a uniform sand subjected to cyclic direct simple shear loading with no initial static bias.

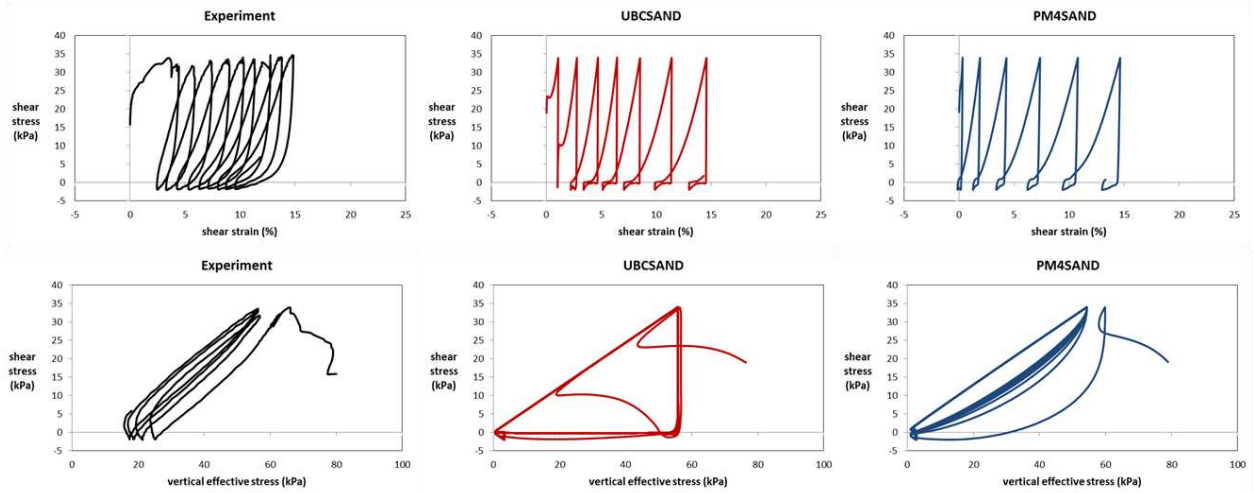

Figure 5. Comparison between experimental and numerical results on a uniform sand subjected to cyclic direct simple shear loading with initial static bias equal to 0.2.

3.2 Laminated Samples subjected to Cyclic Direct Simple Shear loading

A CDSS test without static bias on a laminated sample was reproduced numerically as shown in Figure 7. Using a sample photo (Figure 6a) and X-ray tomography (Figure 2) two 0.6-cm-thick layers of clay were identified within the sample. The numerical model of the CDSS sample, constructed in FLAC2D (Itasca 2011), is shown in Figure 6b. The sand layers were modeled with the calibrated UBCSAND and PM4Sand models based on the liquefaction resistance curve from samples with no laminations. The clay laminations were modeled as Mohr-Coulomb material with an undrained shear strength, Su, of 40 kPa (estimated from adjacent Cone Penetration Test soundings). The close agreement between numerical simulations and experimental results, illustrated in Figure 7, indicates that an accurate numerical simulation in terms of geometry and calibrated effective stress parameters can reproduce the experimental response of laminated sand deposits in terms of liquefaction triggering resistance and post-liquefaction deformations.

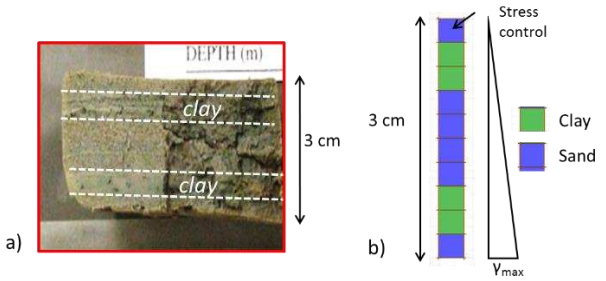

Figure 6. a) Photo of a laminated sample subjected to CDSS testing, b) Numerical model of the laminated sample.

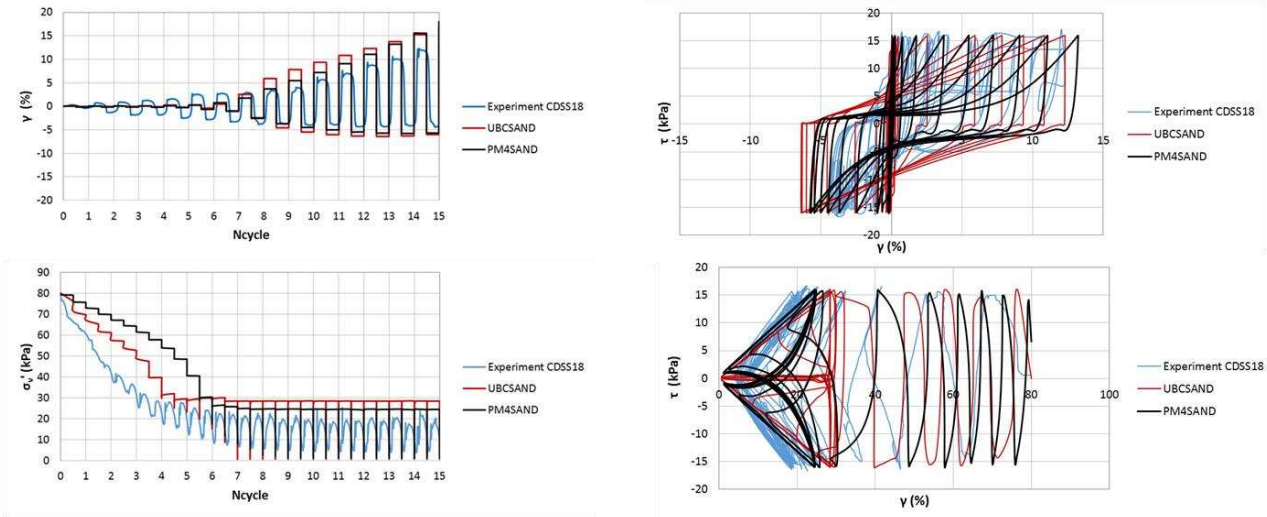

Figure 7. Comparison between experimental and numerical results of a laminated sample (Figure 5) subjected to cyclic simple shear loading.

3.3 Laminated Samples subjected to Cyclic Plane Strain Compression loading

A CTX test on a laminated sample was simulated numerically using PM4Sand to model the sand laminations. Due to limitations regarding the implementation of PM4Sand in FLAC2D (currently restricted to plane strain conditions), the numerical simulation was for cyclic plain strain loading instead of cyclic triaxial loading.

Idealized Models. Initial numerical simulations were performed for a uniform sand sample loaded monotonically under plane strain compression. Subsequently, similar simulations were performed on a laminated sample. The sand layers were assigned similar properties as for the uniform sand sample, while the clay layers were modeled using a total stress model with an undrained shear strength of 40-kPa.

Figure 8 shows the two different models together with the results of undrained monotonic plane strain compressional loading. As shown on the figure, the deformation patterns are different in that the uniform samples (as expected) develop localized shear bands, while the presence of the clay layers, causes distributed shearing and an overall bulged deformation pattern.

Numerical simulations under cycling plane strain compression loading were also conducted to compare the response of a uniform sample with an interlayered sample as shown on Figure 9. Also shown on the figure are: 1) plots of shear strain development within the mesh (the numbers represent the cycle number at which axial strains of about 1.5 percent develop in the element at that location); and 2) the cyclic resistance curves at which liquefaction develops. The numerical results indicate that the presence of the clay laminations tends to: a) increase the cyclic resistance (i.e. an increased number of cycles

to develop liquefaction), and b) tend to inhibit shear localization by distributing shear strains.

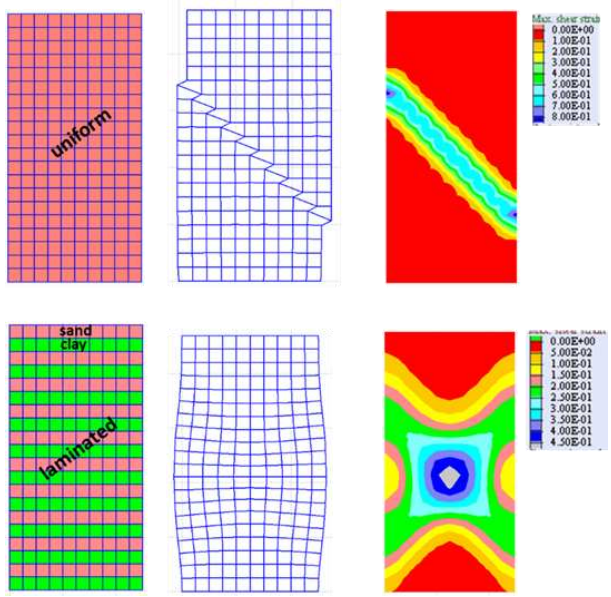

Figure 8. Deformed meshes and contours of shear strain for a specimen consisting of uniform sand (top) and laminated soil with alternating layers of sand and clay (bottom) under monotonic plane strain compression.

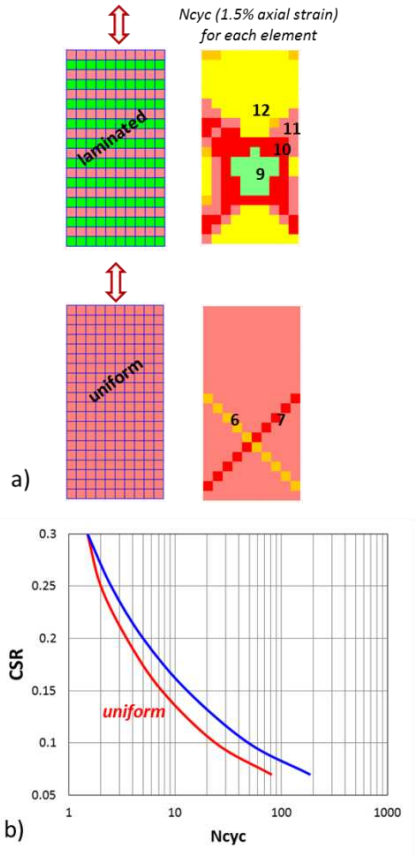

Figure 9. a) Contours of the required number of cycles to cause 1.5% axial strain for a specimen consisting of laminated soil with alternating layers of sand and clay (top) and uniform sand (second plot) under cyclic plane strain compression loading. b) Liquefaction triggering curves.

Sample Models. As a second step, numerical simulations of actual CTX tests on laminated samples were performed. Figure 10a shows the X-ray image and the detailed 2D (i.e. plane strain) numerical model of a laminated sample that was subjected to CTX testing (CSR=0.28). Once again, the sand layers were modeled with the calibrated PM4Sand parameters for uniform sand and the clay laminations were modeled as Mohr-Coulomb material with Su=40 kPa.

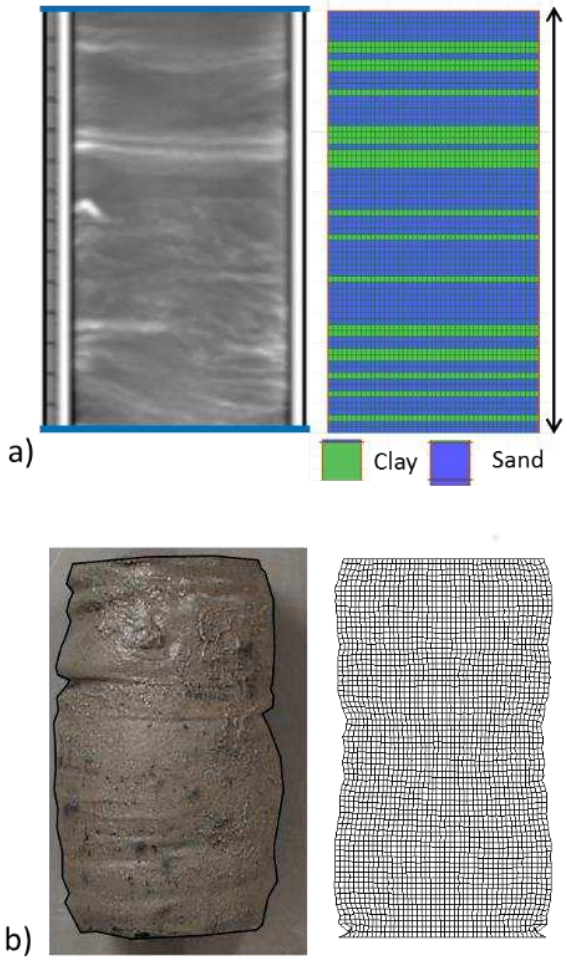

Figure 10. a) X-ray section and numerical grid of a laminated sample subjected to CTX. b) The deformed sample and mesh at the end of the loading.

The deformed shape of the numerical model is compared with the cyclic triaxial sample on Figure 10b, showing somewhat similar characteristics. Figure 11 depicts the development of cyclic strains versus cycles of loading. The axial strains from the simulation were estimated by tracking the change of the sample height and dividing it by its initial height, similar to the measurements made in the laboratory. Both experiment and simulation suggest triggering (1.5% axial strain) at

about 4 to 4-5 cycles. The cyclic responses are also compared in terms of stress-strain plots, and stress paths. In the numerical simulation, the deviatoric stress, q, was measured at the middle top element of the grid, in the sand material.

Although, there are differences between the simulation and the experiment, attributed to the idealization in the configuration of the clay laminations, the different type of loading (plane strain versus triaxial compression) and the simplified modeling of clay as a Mohr-Coulomb material, the overall reasonable comparison of the triaxial tests with the numerical solutions provide some level of confidence in the use of the calibration process and the available numerical tools. Moreover, perhaps the most noteworthy observation is that within highly interlayered materials, or within layers that are not horizontally continuous, the presence of the clay laminations tends to limit the development of strain localization.

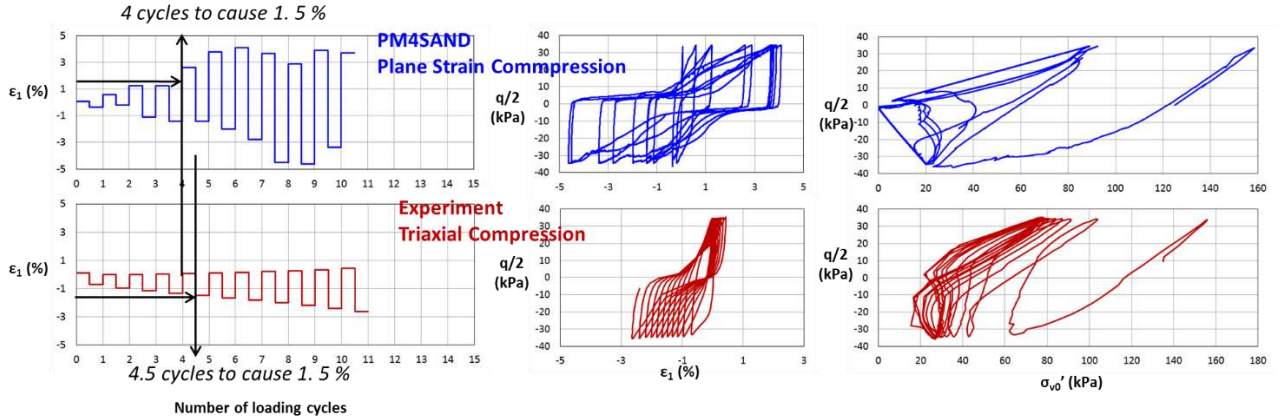

Figure 11. Comparison between numerical and experimental results obtained from cyclic plane strain compression and triaxial compression loading conditions, respectively, on the laminated sample shown on Figure 10.

3.4 1D Site Response of Laminated Soil Deposits

Due to the small size of the sand and clay interlayers (i.e. 10 to 20 cm) explicit modeling of the laminations in 2D numerical models are currently impracticable due to the large computational time required. In an attempt to overcome this limitation one option would be to calibrate the sand constitutive models to the triggering curves interpreted from the cyclic tests on laminated samples (red curve Figure 3). In this case, each element would simulate the composite (macroscopic) behavior of the laminated material rather than the behavior of the sand layers and the clay layers separately. However, the following question arises: would this composite behavior be equivalent to the more realistic explicit modeling of sand and clay interlayers under earthquake loading especially in terms of co-seismic and post-liquefaction deformations?

In order to answer this question, one dimensional nonlinear effective stress site response analyses were performed to investigate the dynamic response of thinly laminated deposits under sloping (i.e. with static bias) ground conditions. A finite difference mesh of a 1D soil column was created using a fine discretization of 20-cm-thick elements for the tidal (laminated) deposits whose total thickness was 5 m (Figure 12).

Sand layers were modeled with PM4Sand and UBCSAND and clay layers were modeled with a Mohr-Coulomb failure criterion in combination with a nonlinear stress-strain behavior. In order to model static bias conditions in 1D site response, the gravity vector was inclined simulating an infinite slope with a static shear stress ratio (α) of 0.1. To compare the dynamic behavior resulting from the use of uniform macroscopic properties with explicit modeling of interlayering, the following cases (shown in Figure 12) were analysed:

- Case A. All elements were modeled as sand without clay laminations (blue CRR curve)
- Case B. Elements were modeled with the composite behavior of laminated samples (red CRR curve).
- Case C. The sand (blue CRR curve) and clay layers of tidal deposits were explicitly modeled.

Figure 13 presents results for the three cases for with-bias conditions (i.e. infinite slope, α =0.1) in the form of profiles of maximum excess pore pressure ratio and maximum lateral displacements at the end of shaking.

In Case A, liquefaction is triggered resulting in a maximum excess pore pressure ratio of 1 throughout the layer. Ground surface lateral displacements on the order of 0.65 m develop at the end of shaking under sloping ground conditions. By contrast, in Case B when the tidal deposits comprise of sand with higher CRR, corresponding to laminated samples, liquefaction is only triggered near the base of the layer for both constitutive models. Maximum lateral displacements at the end of shaking are in the order of 0.43-0.44m, i.e an approximately 30% reduction compared to Case A. In Case C, where the sand and clay laminations are modeled explicitly, maximum lateral displacements at the

end of shaking are similar to those obtained for case B (0.45-0.47 cm), indicating that the presence of clay laminations impedes the development of large deformations due to liquefaction. Maybe most importantly the system dynamic response in Case B where composite elements are used to model the cyclic resistance of laminated samples is quite similar to the system dynamic response of Case C where the sand and clay laminations are modeled explicitly. This provides confidence that composite elements can be used for more complex 2D numerical analyses (with similar soil conditions and shaking levels) to model the behavior of laminated deposits, after appropriate calibration.

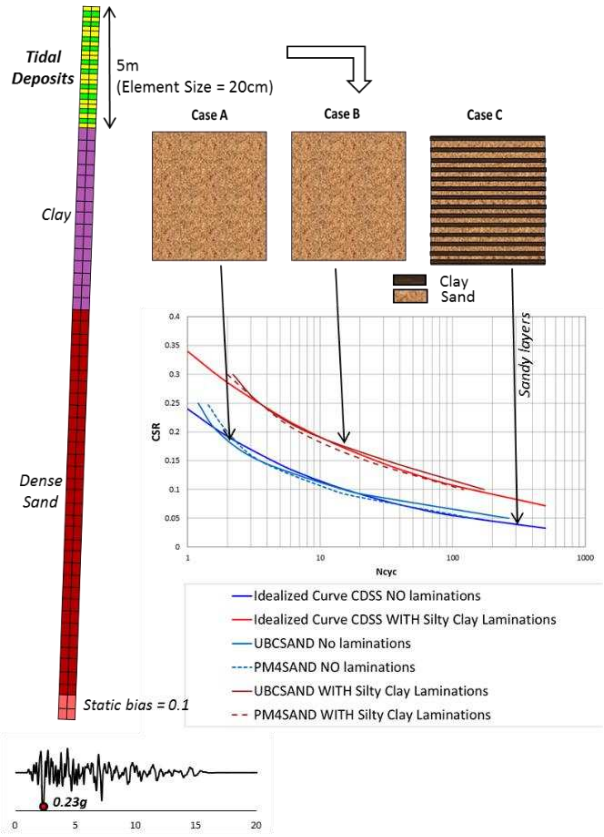

Figure 12. 1D Numerical model and three different configuration of the tidal deposits which are modeled as: A) uniform sand (blue curve), B) uniform sand (red curve) and C) laminated soil with alternating layers of sand (blue curve) and clay.

3.5 Void Redistribution Effects on Laminated Soils

In laminated deposits, the presence of clay interlayers creates permeability contrasts that would inhibit the dissipation of cyclically-induced pore pressures, theoretically resulting in void redistribution and potential strain localization (Tokimatsu et al, 2001; Kamai and Boulanger, 2013). Parametric numerical investigations were performed to evaluate the potential for void redistribution with respect to the thickness of the sand layer. Effective stress nonlinear site response analyses were performed for a 1D profile using a very fine discretization of 5-cm-thick elements to model the tidal (laminated) deposits. In order to study void redistribution effects, the input ground motion were scaled up to ensure that the sand laminations liquefied in all cases analyzed. Additionally, relatively large permeability was used for the sand layers so that void redistribution effects could develop at the end of shaking. Figure 14 shows the cases considered in these sensitivity analyses and presents the results of the parametric investigation in the form of relative density versus depth at the end of shaking. The following are noteworthy:

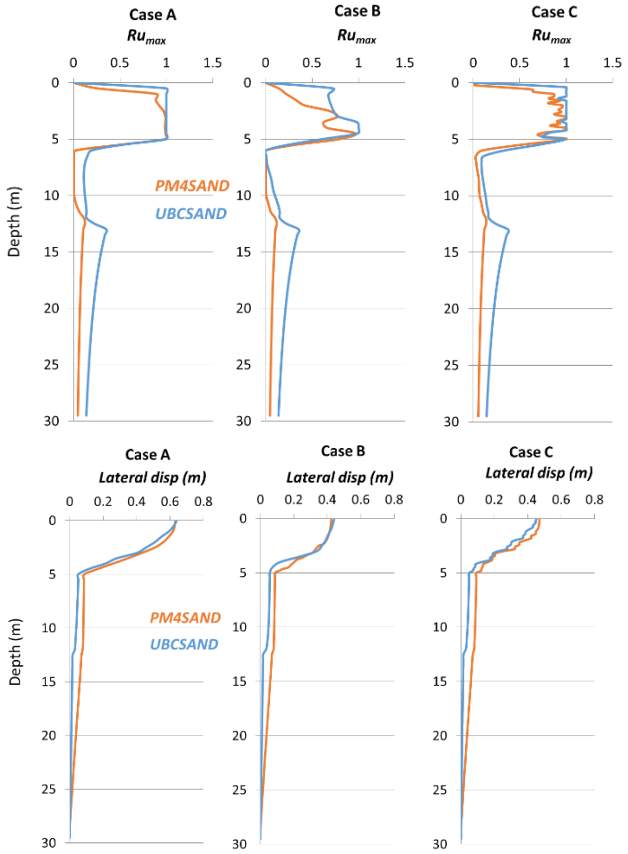

Figure 13. Maximum excess pore pressure ratio (top) and residual lateral displacement (bottom) versus depth and for the three cases presented in Figure 12.

- In Case 1a (left graph) where a uniform sand layer is modeled with no clay layers, at the end of shaking excess pore pressures migrate freely from the bottom part of the unit towards the phreatic surface resulting in densification of the bottom part of layer. Few void redistribution effects are observed in this case, although the layers are densified.
- When a clay layer is present at the top of the sand layer (Case 1b), the clay layer inhibits dissipation and the resulting accumulation of water results in loosening of the sand layer below the clay interface (i.e. void redistribution effects). Densification is still observed at the bottom part of the layer. This is shown on the second graph from

the left where the relative density of the upper part of the tidal deposits layer right below the clay layer reduces to 15-35% whereas it increases close to the bottom of the layer.

- The effect of void redistribution (i.e. shown here through the decrease in relative density) decreases as the thickness of the sand layer decreases. This is observed by comparing the 2nd, 3rd, 4th and 5th graph on Figure 13, where it is shown that relative density at the end of shaking reduces to 35%, 49%, 76% and 95% of its initial value for a 4.5-m-, 0.5-m, 0.25-m- and 0.10-m-thick sand layer, respectively.

The above results help illustrate the mitigating effect of thin clay layers such as would be present in the laminated deposits on the potential for void redistribution. It should be mentioned that the effect of void redistribution not only decreases as the thickness of the sand layer decreases – a finding consistent with experimental and numerical studies by Kulasingam et al. (2004), Sento et al. (2004) and Malvick et al. (2006) – but also when the permeability contrast between the laminations decreases.

4 CONCLUSIONS

Advanced cyclic laboratory tests on uniform and laminated samples and subsequent numerical simulation of tests provided evidence that the presence of clay layers within interlayered sand and clay deposits tends to increase the liquefaction triggering resistance of the overall deposit. In particular, numerical investigations of the behavior of laminated samples under cyclic plane strain compression loading (similar to CTX), indicated that the presence of the clay laminations tends to limit the development of strain localization leading to a wider strain distribution.

1D site response numerical analyses, involving explicit modeling of the sand/clay layers, showed that: i) laminated soils can be modeled as uniform sand materials using advanced constitutive models calibrated to the composite (macroscopic) behavior measured in laboratory tests on laminated samples and ii) void redistribution effects, often considered a source of strain localization tend to be significantly reduced as the thickness of sand lamination decreases, or as the percentage of clay interlayers increases.

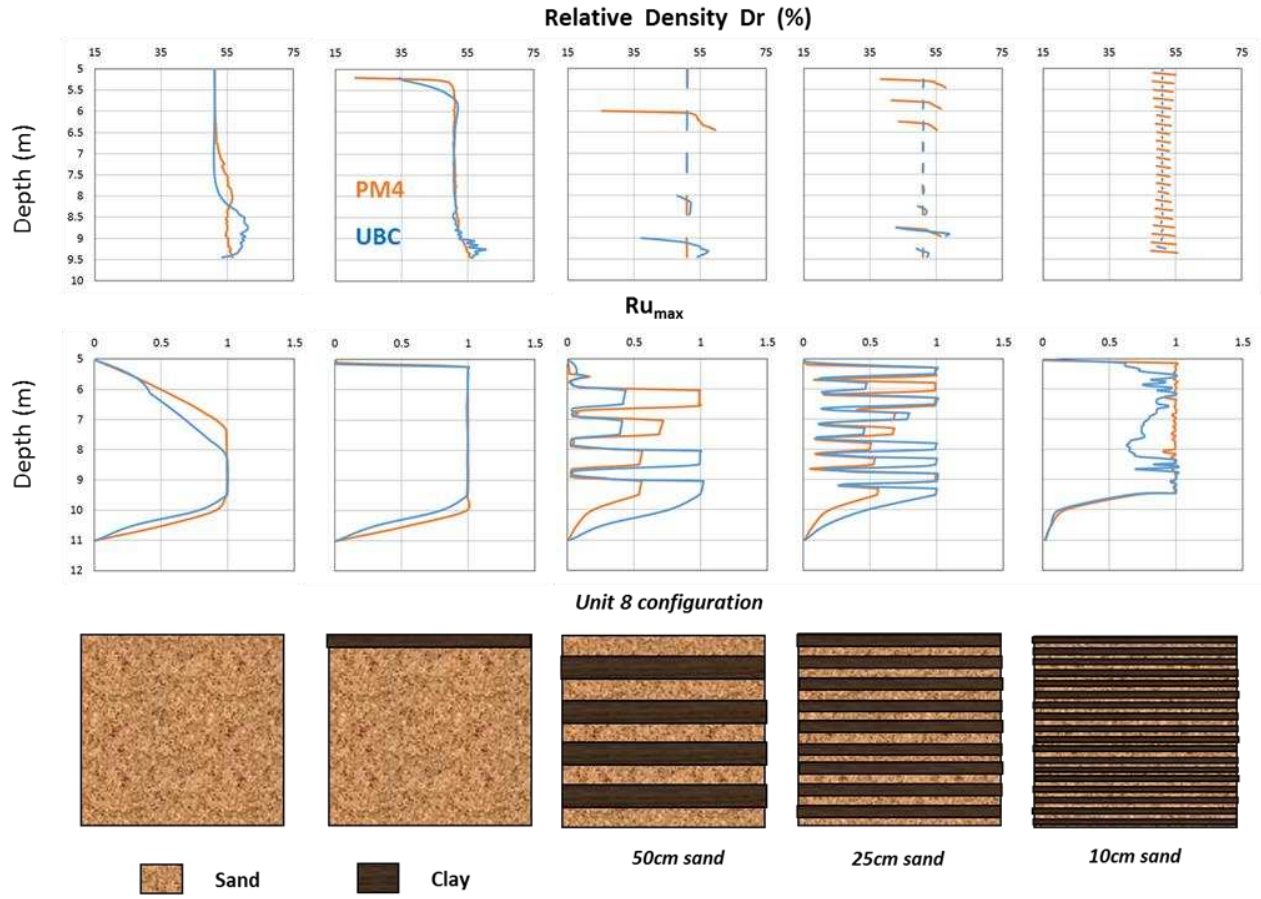

Figure 14. Variation of relative density within sand layers due to void redistribution effects.

5 REFERENCES

Boulanger, R. W., and Idriss I.M. 2014. *CPT and SPT Based Liquefaction Triggering Procedures*, Report No. UCD/CGM-14/01, University of California, Davis, April

Boulanger, R. W., and Ziotopoulou, K. 2013. Formulation of a sand plasticity plane-strain model for earthquake engineering applications. *Journal of Soil Dynamics and Earthquake Engineering,* Elsevier, 53: 254-267.

Beaty, M., and Byrne, P.M., (1998). "An Effective Stress Model for Predicting Liquefaction Behavior of Sand," Proceedings of a Specialty Conference, Geotechnical Earthquake Engineering and Soil Dynamics, ASCE pp. 766-777, Seattle.

Giannakou, A., Travasarou, T., Ugalde, J., Chacko, J., and Byrne, P. (2011), "Calibration Methodology for Liquefaction Problems Considering Level and Sloping Ground Conditions"," 5th International Conference on Earthquake Geotechnical Engineering, Chile.

Idriss I. M., and Boulanger R. W. 2008. *Soil Liquefaction During Earthquakes*, Earthquake Engineering Research Institute

Itasca Consulting Group Inc. 2013. *Fast Lagrangian Analysis of Continua (FLAC2D) version 7.0*

Kamai, R., and Boulanger, R. W. 2013. Simulations of a centrifuge test with lateral spreading and void redistribution effects. *Journal of Geotechnical and Geoenvironmental Engineering*, ASCE, 139(8): 1250-1261.

Kulasingam, R., Malvick, E. J., Boulanger, R. W. & Kutter, B. L. 2004. Strength loss and localization at siltinterlayers in slopes of liquefied sand. *Journal of Geotechnical and Geoenvironmental Engineering,* ASCE, 130: 1192-1202.

Malvick, E. J., Kutter, B. L., Boulanger, R. W., and Kulasingam, R. 2006. Shear localization due to liquefaction-induced void redistribution in a layered infinite slope. *Journal of Geotechnical and Geoenvironmental Engineering,* ASCE, 132(10): 1293-1303.

Moss, R. E. S., Seed, R. B., Kayen, R. E., Stewart, J. P., Youd, T. L., and Tokimatsu, K. (2003). "Field case histories for CPT-based in situ liquefaction potential evaluation." Geoengineering Research Rep. UCB/GE-2003/04.

Sento, N., Kazama, M., Uzuoka, R., Hirofumi Ohmur H., and Makoto Ishimaru, M. 2004. Possibility of post liquefaction flow failure due to seepage. *Journal of Geotechnical and Geoenvironmental Engineering,* ASCE, 130: 707-716.

Tokimatsu, K., Taya, Y., and Zhang, J. M. 2001. 'Effects of pore water redistribution on post-liquefaction deformation of sands. *Proc., 15th Int. Conf. on Soil Mechanics and Geotechnical Engineering*, Balkema, Rotterdam, The Netherlands, 1, 289–292

Youd, T. L., Idriss, I. M., Andrus, R. D., Arango, I., Castro, G., Christian, J. T., Dobry, R., Finn, W. D. L., Harder, L. F., Hynes, M. E., Ishihara, K., Koester, J. P., Liao, S. S. C., Marcuson, W. F., Martin, G. R., Mitchell, J. K., Moriwaki, Y., Power, M. S., Robertson, P. K., Seed, R. B., and Stokoe, K. H. (2001). Liquefaction resistance of soils: summary report from the 1996 NCEER and 1998 NCEER/NSF workshops on evaluation of liquefaction resistance of soils, J. Geotechnical and Geoenvironmental Eng., ASCE 127(10), 817–33.

Ziotopoulou, K., and Boulanger, R. W. 2013. Calibration and implementation of a sand plasticity plane-strain model for earthquake engineering applications. *Journal of Soil Dynamics and Earthquake Engineering*, 53: 268-280.